Romanian Reports in Physics, Vol. 67, No. 4, P. 1288–1299, 2015

Dedicated to
International Year of Light 2015

ANALYSIS OF AN ERBIUM FIBER LASER OPERATED IN PASSIVE Q-SWITCH MODULATED MODE-LOCKING REGIME BY USING AN UN-PUMPED OPTIC FIBER

S. MICLOS[1], D. SAVASTRU[1], R. SAVASTRU[1], I. LANCRANJAN[1]

[1] National Institute of R&D for Optoelectronics INOE 2000, 409 Atomistilor Str., RO-077125, Magurele, Ilfov, Romania
E-mails: dsavas@inoe.ro, miclos@inoe.ro, rsavas@inoe.ro, j_j_f_l@yahoo.com

Received October 1, 2015

Abstract. An analysis of several Ytterbium, Ytterbium/Erbium and Erbium all-fiber laser or using bulk components configurations, CW or pulsed pumped, operated in passive Q-switching, mode-locking and passively self-modulated amplitude mode-locking regimes is presented. The analysis is developed with the purpose of an improved design of fiber lasers dedicated to micro-processing applications.

Key words: Ytterbium, Erbium, fiber laser, passive Q-switch, mode-locking.

1. INTRODUCTION

The main purpose of the paper consists in presenting the first part of simulation results obtained pursuing to an improved design of NIR fiber lasers generating ultrashort pulses in Passive Q-switching (PQsw), Mode-Locking (ML) and passively Q-switched Modulated Amplitude Mode-Locking (MAML) operation regimes used for materials micromachining and glass micro-processing applications [1–12]. High power Q-switched fiber lasers with nanosecond or picosecond pulse durations are of great interest for such applications because compared with conventional bulk solid-sate lasers; fiber lasers have some intrinsic merits and have seen a tremendous growth on research market. One important particular reason for simulating and, on this basis, improving the design of PQsw, ML, MAML fiber or/and all-fiber lasers relies on the quality of their output beam quality which is useful for glass micromachining, specifically bare optic fiber. For example, using fiber lasers with good beam quality and emission wavelength in the NIR spectral range of 1–1.5 μm it is possible to focus the output beam to a spot with ~1μm diameter useful for drilling transverse holes through SM optic fibers or tapered micro channels in glass, aiming to develop a new type of sensors [2, 6–9].

The performed simulation of NIR fiber laser has the scope of developing a software toolbox dedicated to an optimal laser design for micromachining bare SM optic fiber. Because the investigated domain of fiber laser operated in PQsw, ML

and MAML regimes is a large one, the paper is structured into two parts: the first one dealing with PQsw operation regime, with emphasize on Yb fiber laser and the second one dealing with the other two laser operation technique, ML and MAML, with emphasize on Yb-Er and Er fiber lasers.

2. GENERAL CONSIDERATIONS

As mentioned in Section 1, compared with conventional bulk solid-sate lasers the fiber ones have excellent functional properties, including thermal ones due to the fact that their high surface areas to volume ratios allow efficient thermal dissipation and usually they do not need active cooling [11–14]. In addition, the fiber's wave guiding properties reduce thermal distortion of the beam and allow superior beam quality making possible the focusing of their output beams to ~1μm spots. An important improvement in fiber laser consists in using cladding pump scheme for coupling of higher pump powers into the fiber lasers [11–19].

Soon after the first reports about fiber laser, as in the case of bulk solid state lasers, because of applications related practical reasons, how to control the time shape of fiber laser output was under intensively investigation, meaning research on Q-switching and mode-locking techniques [16–18, 20]. As in the case of bulk solid state laser, two main possibilities were considered: the ones based on using electro-optical effects and the others relying on self-induced nonlinearity transmission of laser resonator components. The light guidance characteristic of optic fiber plays an important role in this research because the design of all-fiber laser experimental setups becomes possible, implying the ease of laser components interconnectivity [20, 26]. Active q-switching devices were considered, including all-fiber laser setups [22–24] but the main effort was focused on passive bulk crystal or doped fiber Q-switching devices. Compared with active Q-switching, passively Q-switched fiber lasers have the advantages of high efficiency, simplicity, compactness, potentially lower cost and might be used more easily in an all-fiber design.

Many passively Q-switched DC or pulsed pumped Yb, Er and Yb-Er fiber lasers have been reported to date. The bulk crystal saturable absorbers (SA) as passive Q-switches have also been applied to fiber lasers. Fiber lasers having Yb, Er, Tm or Nd doped or Yb-Er co-doped optic fibers as active media were passively Q-switched using SA made of Cr^{4+}:YAG [26–29], Cr^{2+}:ZnSe [30, 31], Co^{2+}:ZnSe or Co^{2+}:$MgAl_2O_4$ [32, 33] bulk crystals. Semiconductor saturable mirror (SESAM) was also investigated as passive Q-switching devices suitable for an all-fiber design, but it is vulnerable to high optical power, thus limiting the output power. Of special interest are SA made of spliced optic fiber doped Sm, Cr, Tm, Ho ions or with un-pumped ions as the active medium (Yb, Er) or, somehow as an extreme case, using excess long fiber active medium having a segment where pumping is insufficient to create population inversion [19, 34–40].

3. FIBER LASER PASSIVE Q-SWITCHING THEORY

The theory of passively Q-switched fiber laser using bulk or fiber SA devices is similar in many aspects to the one applied to bulk solid state lasers [11, 41–48]. A major difference arose as a result of the fact that the optic fiber has a length several orders of magnitude larger than its transverse dimensions implying that two arguments, a position coordinate and time have to be used in definition of a laser rate equation simulation model. This implies that the phenomena inside a PQsw operated fiber laser can be accurately simulated using a system of coupled partial differential rate equations. The simulation model has to represent the transport of pump or signal laser radiation powers along the optic fiber and, coupled with them, the time variation of fixed active or SA ions excited to the upper laser level [49, 50]. The guiding characteristic of optic fibers has importance concerning the role of amplified spontaneous emission (ASE) [51, 52]. The developed model is a Travelling Wave one, being of finite difference time domain (FDTD) type. The accuracy of the simulation model depends on defining the initial and boundary conditions of the coupled partial differential rate equations system. The boundary conditions simply describe coupling of the pump power to one or both ends of the active fiber medium (with an initial specified value) and pump and laser signal propagation into fiber laser resonator. The initial conditions can be defined as zero values for pump and laser signal powers inside fiber laser resonator, for population inversion and for saturable absorber upper level population densities. It is worth to mention that all-fiber laser designs implies the use of FBG's (fiber Bragg grating) as reflectors implying that their peak reflection wavelength defined with fine bandwidth (< 0.5 nm) has to be considered. In Figs. 1–4 four of the most reported in literature as used passively Q-switched fiber laser experimental setups are schematically represented. In Fig. 1 is represented the case of a bulk crystal saturable absorber used into a laser resonator having flat reflectivity variation *versus* laser signal wavelength. In Figs. 2–4, the presented all-fiber laser setups using FBG's reflectors.

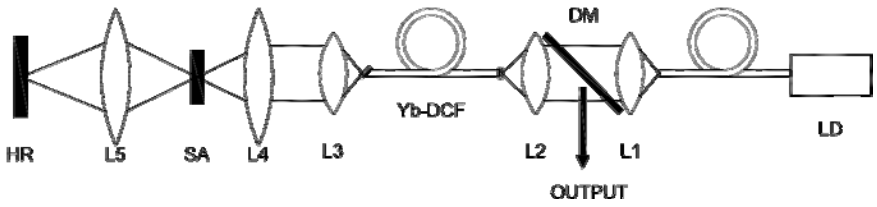

Fig. 1 – Configuration diagram of Yb fiber laser using a Cr^{4+}:YAG bulk crystal Q-switching device. LD – CW or pulsed pumping laser diode; Yb-DCF – Yb doped double clad fiber active medium; SA – Cr4+:YAG crystal passive Q-switching device; L1, L2, L3, L4 and L5 convex lenses used for coupling pump power to the Yb-DCF and laser radiation through the SA; HR – plane high reflectivity mirror; DM – dichroic mirror used as laser output coupler.

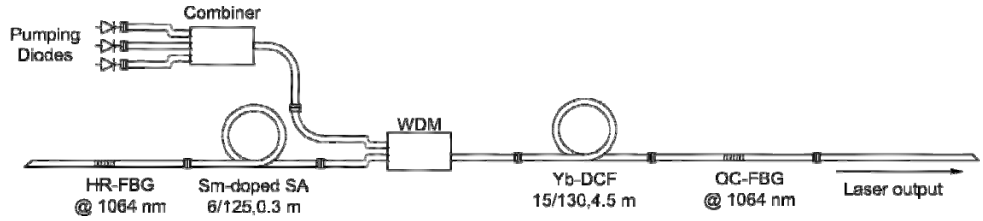

Fig. 2 – Configuration diagram of passively Q-switched all-fiber laser using a Sm doped fiber Q-switching device. Pumping Diodes – CW or pulsed pumping laser diodes; Combiner and WDM are coupling the pump power into a double clad Yb doped fiber used as active medium; Yb-DCF – Yb doped double clad fiber active; Sm-doped SA – Sm doped fiber; HR-FBG – high reflectivity FBG used as rear laser mirror; OC-FBG – low reflectivity FBG used as laser output coupler.

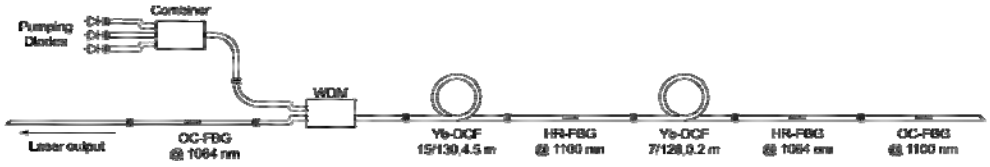

Fig. 3 – Configuration diagram of passively Q-switched all-fiber laser using un-pumped Yb fiber as Q-switching device. Pumping Diodes – CW or pulsed pumping laser diodes; Combiner and WDM are coupling the pump power into a double clad Yb doped fiber used as active medium; Yb-DCF – Yb doped double clad fiber active medium; Yb-DCF 7/128,0.2 m – Yb doped SM fiber Q-switch device; HR-FBG@1064nm – high reflectivity FBG used as rear laser mirror; OC-FBG@1064nm – low reflectivity FBG used as laser output coupler; HR-FBG@1100nm – high reflectivity FBG connected with Yb-SA; OC-FBG@1100nm – low reflectivity FBG connected with Yb-SA.

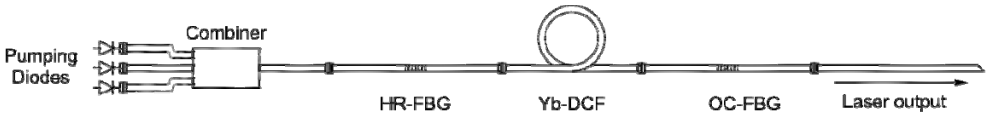

Fig. 4 – Configuration diagram of passively Q-switched all-fiber laser using an "excess" of fiber. Pumping Diodes – CW or pulsed pumping laser diodes; Combiner and WDM are coupling the pump power into a double clad Yb doped fiber used as active medium; Yb-DCF – Yb doped double clad fiber active medium; HR-FBG – high reflectivity FBG used as rear laser mirror; OC-FBG – low reflectivity FBG used as laser output coupler.

The coupled rate partial differential equations system, the essence of the developed simulation model can be grouped into several packages, as it follows:

Active medium gain equations are:

$$N_0 = N_1(t) + N_2(t) \tag{1}$$

$$\frac{\partial N_2(x,t)}{\partial t} = \frac{\Gamma_p \lambda_p}{hcA_{co}}\left[\sigma_{\alpha p} N_1(x,t) - \sigma_{ep} N_2(x,t)\right] P_p^-(x,t) + \\ + \sum_k \frac{\Gamma_k \lambda_k}{hcA_{co}}\left[\sigma_{\alpha k} N_1(x,t) - \sigma_{ek} N_2(x,t)\right]\left(P_k^+(x,t) + P_k^-(x,t)\right) - \frac{N_2(x,t)}{\tau}, \tag{2}$$

$$\mp \frac{\partial P_p^-(x,t)}{\partial x} \pm \frac{1}{v_p}\frac{\partial P_p^-(x,t)}{\partial t} = \\ = \Gamma_p\left[\sigma_{ep} N_2(x,t) - \sigma_{\alpha p} N_1(x,t)\right] P_p^-(x,t) - \alpha_p P_p^-(x,t), \tag{3}$$

$$\pm \frac{\partial P_k^\pm(x,t)}{\partial x} + \frac{1}{v_k}\frac{\partial P_k^\pm(x,t)}{\partial t} = \\ = \Gamma_k\left[\sigma_{ek} N_2(x,t) - \sigma_{\alpha k} N_1(x,t)\right] P_k^\pm(x,t) - \alpha_k P_p^\pm(x,t) + N_2(x,t)\xi_k, \tag{4}$$

where: N_0 is the doping concentration in the gain fiber, N_1 and N_2 are the ground and excited state population densities into fiber active medium, P_p^+ is the pump power (the superscript '±' corresponds to the forward and backward propagations, respectively), $P_k^\pm(x,t)$ represents the power of the laser signal propagating backward or forward, λ_p is the pump wavelength, λ_k is the indexed ASE wavelength, σ_{ap}, σ_{ep}, σ_{ak}, σ_{ek} and are the absorption and emission cross-sections for the pump wavelength and indexed signal wavelength, Γ_p and Γ_k are the power confinement factor for the pump and the emission wavelengths, α_p and α_k are the dissipative optical loss for the pump and the emissions, v_p and v_k are the group velocities of the pump and the laser signal, τ is the active ions excited state lifetime, A_{co} is the area of the fiber active medium core, h is the Planck constant, c is the speed of the light, M is the number of transverse modes (2 for LP_{01} single-mode), $\Delta\lambda_k$ is the active ions (Yb in this case) fluorescence bandwidth and ξ_k represents the spontaneous emission coefficient defined as

$$\xi_k = M\Gamma_k \sigma_{ek} \frac{hc^2}{\lambda_k^3}\Delta\lambda_k. \tag{5}$$

Saturable absorber equations are:

$$N^{sa} = N_1^{sa}(t) + N_2^{sa}(t) \tag{6}$$

$$\frac{\partial N_2^{sa}(z,t)}{\partial t} = \sum_k \frac{\lambda_k}{hcA_{sak}(z)}\sigma_{gsak} N_1^{sa}(z,t)\left[P_{sak}^+(z,t) + P_{sak}^-(z,t)\right] - \frac{N_2^{sa}(z,t)}{\tau_{sa}} \tag{7}$$

$$\pm\frac{\partial P_{sak}^{\pm}(z,t)}{\partial z}+\frac{1}{v_{sa}}\frac{\partial P_{sak}^{\pm}(z,t)}{\partial t}= \\ =\left[-\sigma_{gsak}N_2^{sa}(z,t)-\sigma_{esak}N_2^{sa}(z,t)\right]P_{sak}^{\pm}(z,t)+\alpha_{sa}P_{sak}^{\pm}(z,t), \tag{8}$$

where: N_0 is the doping concentration of the saturable absorber, N_1^{sa} and N_2^{sa} are the ground and excited state population densities, σ_{gsak}, σ_{esak} are the absorption cross-sections for the indexed signal wavelength from the saturable absorber ground state and the first excited state, $P_{sak}^{\pm}(x,t)$ is the power of the laser signal propagating backward or forward in SA, respectively, τ_{sa} is the saturable absorber ions excited state lifetime.

Saturable absorber laser signal propagation equations in the bulk crystal case:

$$v_{sa}=\frac{c}{n_{sa}} \tag{9}$$

$$A_{sak}(z)=\pi\omega_{sak}^2(z) \tag{10}$$

$$\omega_{sak}(z)=\omega_{sa0k}(z)\sqrt{1+\left(\frac{z}{z_0}\right)^2} \tag{11}$$

$$z_0=\frac{\pi\omega_{sa0k}^2 n_{sa}}{\lambda_k} \tag{12}$$

where: v_{sa} is the group velocity of the laser signal in saturable absorber, n_{sa} is the saturable absorber refractive index, ω_{sak}^2 is the beam diameter in the bulk saturable absorber corresponding to laser signal with wavelength λ_k, z_0 is the Rayleigh laser beam parameter, z is the depth coordinate inside saturable absorber.

Laser beam propagation equations in the optic fiber:

$$\Gamma_p=\left(\frac{d_{core}}{d_{clad}}\right)^2 \tag{13}$$

$$\Gamma_k=1-\exp\left[-\frac{1}{2}\left(\frac{d_{core}}{\omega}\right)^2\right] \tag{14}$$

$$V=\frac{2\pi d_{core}NA}{2\lambda_k} \tag{15}$$

$$\omega = \frac{d_{core}}{2}\left(0.65 + \frac{1.619}{\sqrt{V^3}} + \frac{2.879}{V^6}\right), \tag{16}$$

where: *NA* is the optic fiber numerical aperture, ω is the beam diameter in the bulk saturable absorber corresponding to laser signal with wavelength λ_k.

Equation defining the *border conditions*:

$$P_p^-(L,t) = P_0 \tag{17}$$

$$P_k^-(L,t) = P_k^+(L,t)\cdot R_{oc} \tag{18}$$

$$P_{output-k}(t) = P_k^+(L,t)\cdot(1-R_{oc}) \tag{19}$$

$$P_{sak}^-(0,t) = P_k^-(0,t)\cdot(1-\eta) \tag{20}$$

$$P_{sak}^+(-L_{sa},t) = P_{sak}^-(-L_{sa},t)\cdot R_{HR} \tag{21}$$

$$P_k^+(0,t) = P_{sak}^+(0,t)\cdot(1-\eta), \tag{22}$$

where: P_0 is the pump power injected into the fiber active medium, η is a radiation coupling factor related to the laser radiation losses at the ends of the optic fiber, R_{oc} and R_{HR} are the reflectivity of output coupler and of rear mirror forming the fiber laser resonator, 0 and L represents the ends of the optic fiber ends, $P_{output\text{-}k}$ is the laser output power at wavelength λ_k. It is worth to notice that the border conditions include the ones referring to bulk or fiber passive Q-switching devices, *i.e.* defining spatial coordinates of the SA fiber ends or considering the bulk crystal saturable absorber as a point because of its negligible length. Among the border conditions are the ones representing the reflectivity of fiber laser resonator mirrors.

4. SIMULATION RESULTS

In Figs. 5–7 are presented the simulation results obtained in the case of an all-fiber laser as described in Fig. 2 using a Sm doped optic fiber (0.3 m length, core of 6 μm, cladding of 125 μm) as saturable absorber. The active medium is formed by an Yb doped double clad fiber of 4.5 m length and having a core of 15 μm diameter and cladding of 130 μm diameter. The FBG's forming the all-fiber laser resonator have peak reflectivity wavelength of 1064 nm and a bandwidth of 0.3 nm. HR-FBG has 0.99 reflectivity and OC-FBG is considered as having 0.04 reflectivity. In Fig. 5 are presented the laser beam diameter variations in active fiber and saturable absorber optic fibers *vs*. laser signal wavelength. In Fig. 6 are

presented the V-numbers of active fiber and saturable absorber optic fibers variations *vs*. laser signal wavelength. In Fig. 7 the output laser signal power time-shape is presented for a CW pump power of 70W. The estimated laser pulses rate is 95 kHz. Laser pulses FWHM time-width is estimated at 2.75 μs. The peak power of output laser pulses is estimated at 325 W. The simulated results are in fairly good agreement with experimental ones reported in literature.

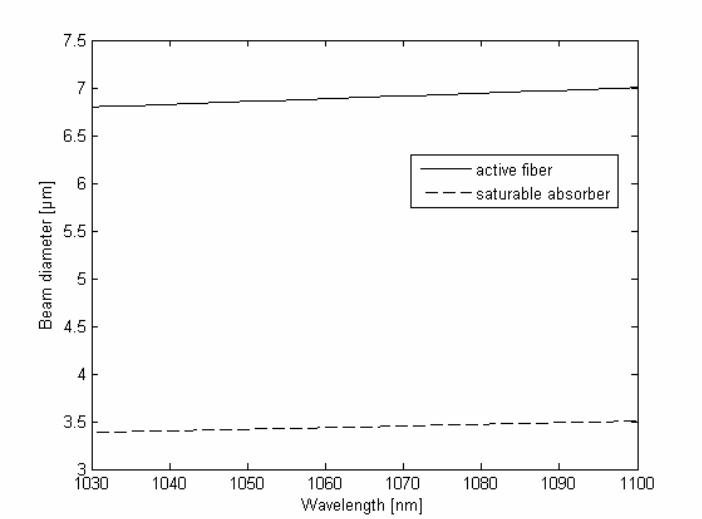

Fig. 5 – Passively Q-switched all-fiber laser incorporating a Sm doped fiber as Q-switching device. Beam diameter of active fiber and saturable absorber *vs*. wavelength.

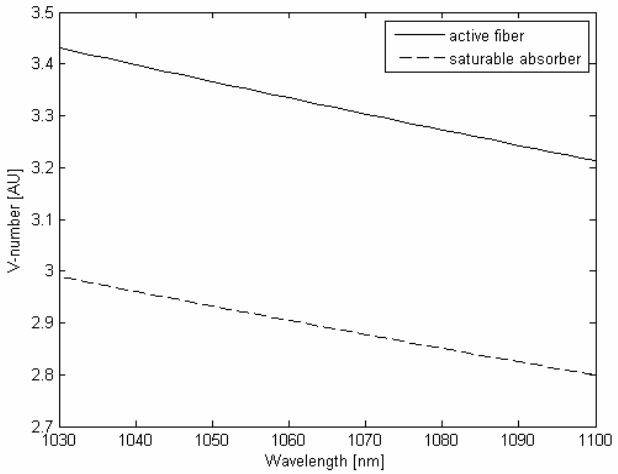

Fig. 6 – Passively Q-switched all-fiber laser incorporating a Sm doped fiber as Q-switching device. V-number of active fiber and saturable absorber *vs*. wavelength.

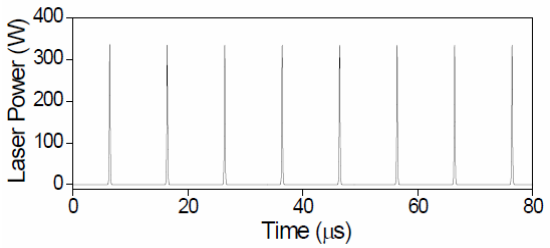

Fig. 7 – Passively Q-switched all-fiber laser incorporating a Sm doped fiber as Q-switching device. Laser power *vs*. time.

In Figs. 8–10 are presented the simulation results obtained in the case of an all-fiber laser as described in Fig. 4 using an "excess" of Yb doped fiber.

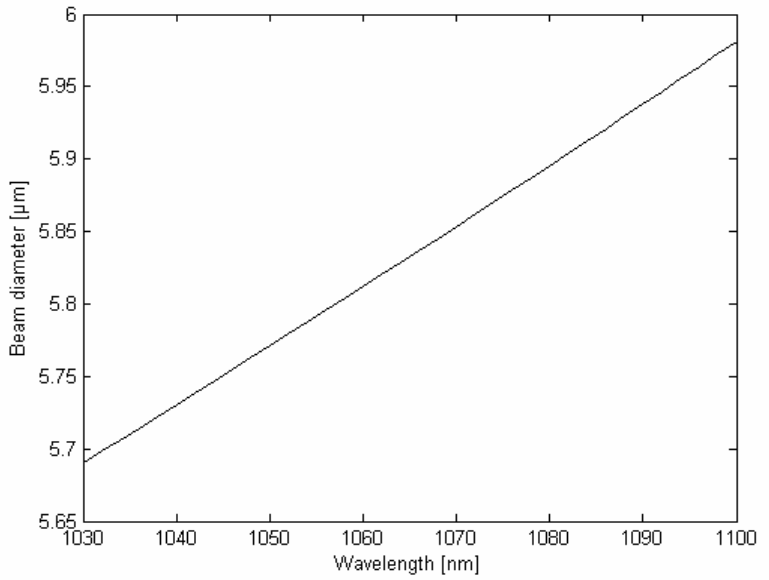

Fig. 8 – Passively Q-switched all-fiber laser using an "excess" of fiber. Beam diameter of active fiber and saturable absorber *vs.* wavelength.

In Fig. 8 is presented the laser beam diameter variations in active fiber *vs.* laser signal wavelength. In Fig. 9 are presented the variations of V-numbers of active fiber *vs*. laser signal wavelength. In Fig. 10 the output laser signal power time-shape is presented for a CW pump power of 70 W. The estimated laser pulse rate is 98.5 kHz. Laser pulses FWHM width is estimated at 0.85 μm. The peak power of output laser pulses is estimated at 515 W. The simulated results are in fairly good agreement with experimental ones reported in literature.

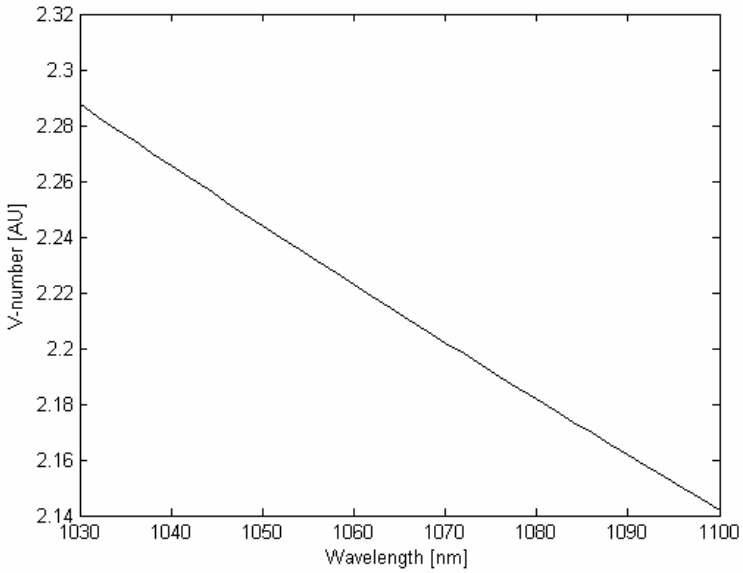

Fig. 9 – Passively Q-switched all-fiber laser using an "excess" of fiber. V-number of active fiber and saturable absorber *vs.* wavelength.

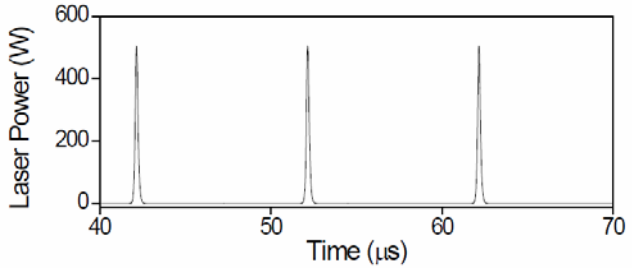

Fig. 10 – Passively Q-switched all-fiber laser using an "excess" of fiber. Laser power *vs.* time.

5. CONCLUSIONS

The main task assumed by the authors when starting the development of a simulation model of passively Q-switched NIR fiber lasers consists in obtaining a set of computer toolboxes which allow an improved design of such lasers to be used in glass and optic fiber micro-processing. Beam diameter, V-number and laser power were determined for an all-fiber laser incorporating a Sm doped fiber as Q-switching device and for an all-fiber laser using an "excess" of fiber, representing such a toolbox.

REFERENCES

1. Rafael R. Gattass, Eric Mazur, Nat. Phot., **2**, 219 (2008).
2. Huan Huang, Lih-Mei Yang, Jian Liu, Opt. Eng., **53**, 051513 (2014).
3. D. Hwang *et al*., Appl. Phys. A: Mater. Sci. Proc., **79**, 605 (2004).
4. M. Bhuyan *et al*., Opt. Expr., **18**, 566 (2010).
5. X. Zhao, Y. C. Shin, Appl. Phys. A: Mater. Sci. Proc., **104**, 713 (2011).
6. S. Darvishi, T. Cubaud, J. P. Longtin, Opt. Las. Eng., **50**, 210 (2011).
7. Y. Jung, G. Brambilla, D. J. Richardson, Opt. Expr., **17**, 5273 (2009).
8. R. An *et al*., Opt. Expr., **13**, 1855 (2005).
9. Y. Bellouard *et al*., Opt. Expr., **12**, 2120 (2004).
10. A. Marcinkevicius *et al*., Opt. Lett., **26**, 277 (2001).
11. O. G. Okhotnikov, *Fiber Lasers*, Wiley-VCH, Weinheim, 2012.
12. J. Swiderski *et al*., Opt. Express, **12**, 3554 (2004).
13. K. Lu, N. K. Dutta, J. Appl. Phys., **91**, 576 (2002).
14. R. Paschotta *et al*., IEEE J. Q. Electron., **33**, 1049 (1997).
15. Y. Wang, X. Chang-Qing, Appl. Opt., **45**, 2058 (2006).
16. J. A. Alvarez-Chavez *et al*., Opt. Lett., **25**, 37 (2000).
17. C. C. Ranaud *et al*., IEEE J. Q. Electron., **37**, 199 (2001).
18. A. Piper *et al*., Electron. Lett., **40**, 928 (2004).
19. T.-Y. Tsai *et al*., Opt. Lett. **34**, 2891 (2009).
20. R. Chi, K. Lu, S. Chen, Microwave Opt. Technol. Lett., **36**, 170 (2003).
21. V. N. Filippov, A. N. Starodumov, A. V. Kiryanov, Opt. Lett., **26**, 343 (2001).
22. N. A. Russo *et al*., Opt. Comm., **210**, 361 (2002).
23. P. Perez-Millan *et al*., Opt. Express, **13**, 5046 (2005).
24. M. Delgado-Pinar *et al*., Opt. Express, **14**, 1106 (2006).
25. A. S. Kurkov, Laser Phys. Lett., **8**, 335 (2011).
26. M. Laroche *et al*., IEEE Photon. Technol. Lett., **18**, 764 (2006).
27. J. Y. Huang *et al*., Opt. Expr., **15**, 473 (2007).
28. C. Y. Lo *et al*., Opt. Lett., **30**, 129 (2005).
29. L. Pan *et al*., IEEE Photon. Technol. Lett., **19**, 1979 (2007).
30. F. Z. Qamar, T. A. King, Opt. Comm., **248**, 501 (2005).
31. V. N. Philippov *et al*., Proc. SPIE, **5335**, 8 (2004).
32. V. N. Philippov *et al*., IEEE Photon. Technol., Lett. **16**, 57 (2004).
33. V. N. Filippov *et al*., Opt. Lett. **26**, 343 (2001).
34. B. Wu, P. L. Chu, IEEE Phot. Technol. Lett., **8**, 230 (1996).
35. A. A. Fotiadi *et al*., Proc. of CLEO/Europe, **29B**, CJ2–3 (2005).
36. T.-Y Tsai *et al*., Opt. Expr., **18**, 23523 (2010).
37. S. W. Moore *et al*., Opt. Expr., **20**, 3778 (2012).
38. D. B. S. Soh, S. E. Bisson *et al*., Opt. Lett., **36**, 2536 (2011).
39. A. A. Fotiadi *et al*., Proc. of CLEO/QELS/PhAST, **15**, CMC4 (2007).
40. A. A. Fotiadi *et al*., Proc. of CLEO/Europe, CJ3–5 (2009).
41. J. Y. Huang *et al*., Appl. Opt., **47**, 2297 (2008).
42. Y. F. Chen, Y. P. Lan, H. L. Chang, IEEE J. Q. Electron., **37**, 462 (2001).
43. Walter Koechner, Michael Bass, *Solid-state lasers*, Springer New York, 2003.
44. J. J. Degnan, IEEE J. Q. Electron., **25**, 1890 (1989).
45. D. Marcuse, IEEE J. Q. Electron., **29**, 2390 (1993).
46. I. Lancranjan, S. Miclos, D. Savastru, J. Opt. Adv. Mat., **12**, 1636 (2010).

47. I. I. Lancranjan, D. Savastru *et al*., Proc. SPIE, **8547**, 854712 (2012)
48. D. Savastru, A. Vlase *et al*., U. P. B. Sci. Bull. – Ser. A, **73**, 167 (2011).
49. J. W. Thomas, *Numerical partial differential equations: finite difference methods*. *Vol. 1*, Springer New York, 1995.
50. R. Courant, D. Hilbert, *Methods of Mathematical Physics*, Vol. 1, Interscience New York, 1953.
51. Huang, De X. Huang, JOSA B, **21**, 1479 (2004).
52. S. Kuck *et al*., Phys. Rev. B, **51**, 17323 (1995).